NANO LETTERS

Letter

pubs.acs.org/NanoLett

Bright UV Single Photon Emission at Point Defects in *h*-BN

Romain Bourrellier, Sophie Meuret, Anna Tararan, Odile Stéphan, Mathieu Kociak, Luiz H. G. Tizei, and Alberto Zobelli*

Laboratoire de Physique des Solides, Univ. Paris-Sud, CNRS UMR 8502, F-91405, Orsay, France

ABSTRACT: To date, quantum sources in the ultraviolet (UV) spectral region have been obtained only in semiconductor quantum dots. Color centers in wide bandgap materials may represent a more effective alternative. However, the quest for UV quantum emitters in bulk crystals faces the difficulty of combining an efficient UV excitation/detection optical setup with the capability of addressing individual color centers in potentially highly defective materials. In this work we overcome this limit by employing an original experimental setup coupling cathodoluminescence within a scanning transmission electron microscope to a Hanbury–Brown–Twiss intensity interferometer. We identify a new extremely bright UV single photon emitter (4.1 eV) in hexagonal boron nitride. Hyperspectral cathodoluminescence maps show a high spatial localization of the emission (~80 nm) and a typical zero-phonon line plus phonon replica spectroscopic signature, indicating a point defect origin, most likely carbon substitutional at nitrogen sites. An additional nonsingle-photon broad emission may appear in the same spectral region, which can be attributed to intrinsic defects related to electron irradiation.

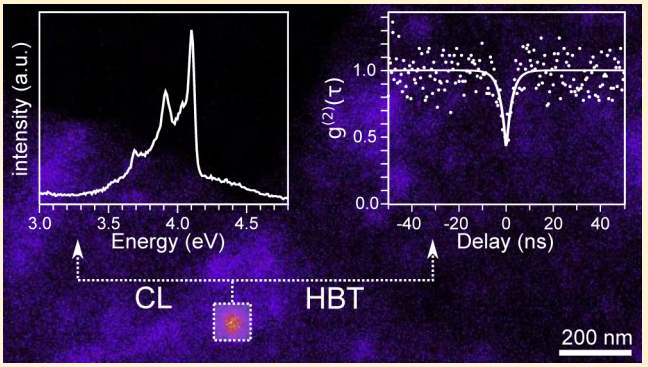

KEYWORDS: *Boron nitride, point defects, single photon source, ultraviolet, cathodoluminescence, scanning transmission electron microscopy*

Optics with individual photons are playing a key role in the route toward future quantum computing and information-processing technologies. For useful applications, single-photon emitter (SPE) systems must be stable over a long time, easy to set up, and preferably composed of a cheap material. Therefore, there is an active research area focused on finding new SPEs, with different emission wavelengths and larger emission rates, and possibly excited by means other than a laser,[1] such as an electrical current (electroluminescence)[2] or fast electrons (cathodoluminescence, CL).[3]

Thus, far, semiconductor quantum dots and color centers in diamond and silicon carbide[4,5] have offered a solid-state platform for optically stable, room-temperature single quantum emitters in the visible range. In recent years low-dimensional layered semiconductors have appeared as new promising optical materials, and very recently single-photon sources have been described in transition metal dichalcogenides[6−10] and hexagonal boron nitride (*h*-BN).[11−14]

Quantum communication is usually performed by sending (single) photons down optical fibers, but free-space links have been identified as a viable alternative.[15,16] The UV spectral range presents the advantage of a very limited solar illumination background, permitting optical communication in daylight.[17] Up to now only sparse reports of UV-SPE have been made, mainly due to technical difficulties in growing wide bandgap nanostructures with SPE character. UV single-photon sources operating at 200 K have been obtained using GaN and InGaN quantum dots,[18−20] but the synthesis of this class of nanostructures remains challenging, and room-temperature efficiency remains low with the recent exception of GaN dots in AlN nanowires.[21] High-energy single-photon sources can in principle be obtained also through photon upconversion techniques,[22] but their application to the UV spectral range has not yet been reported.

Color centers in wide bandgap materials may represent a more accessible route toward room temperature UV-SPEs. Recently, *h*-BN has emerged as a promising candidate for optoelectronic applications due to its strong UV emissions, which are stable at room temperature.[23−25] Whereas high-quality crystals have a luminescence dominated by a sharp 5.75 eV line,[26] stacking faults induce additional high-energy excitons in the 5.4−6.2 eV energy range.[27] Furthermore, very recently it emerged that phonons play a key role in defining the de-excitation channels for both bulk and stacking-fault-bound excitons.[28,29] Additional strong features in the UV spectral region have been associated with extrinsic defects,[30] but the quantum nature of these emissions has not been explored so far.

Indeed, the quest for UV quantum emitters in bulk crystals faces the difficulty of combining an efficient UV excitation/detection optical setup with the capability of addressing individual color centers in potentially highly defective materials.

Received: April 1, 2016
Revised: June 9, 2016
Published: June 14, 2016

DOI: 10.1021/acs.nanolett.6b01368
Nano Lett. 2016, 16, 4317−4321

This problem can be overcome by employing a fast electron beam, which can be focused in a subwavelength spot size, as the illuminating radiation. Therefore, the integration of a CL system into a scanning transmission electron microscope (STEM) allows a spatial selectivity as high as a few nanometers[31] while providing a relatively easy access to the UV spectral range.[27,32] The CL signal can then be guided into a light intensity Hanbury–Brown–Twiss (HBT) interferometer.[33] The potential nonclassical nature of highly localized emissions can be easily demonstrated by the appearance of an antibunching signature in the second-order correlation function, $g^{(2)}(\tau)$. This original experimental setup has already been successfully applied to the study of NV centers in nanodiamonds,[3,34] but the same methodology can be easily employed in the quest for unknown single photon emitters in new optical materials.

In this work we employ an original CL+HBT system to identify a new UV-SPE in *h*-BN that can be attributed to native crystal point defects thanks to the high spatial localization of the emission in the CL maps and a typical zero-phonon line plus phonon replica spectroscopic signature. This emission may be accompanied by a broader non SPE emission, which we attribute to intrinsic defects.

The setup used in this work, combining high-angle annular dark-field (HAADF) imaging, filtered CL imaging, CL-HBT, and hyperspectral imaging in a STEM is detailed in the methods section and in ref 3. In Figure 1.a we present an HAADF image of several chemically exfoliated *h*-BN flakes; the image contrast homogeneity indicates the large extension of flat regions. Figure 1b is the corresponding midbandgap emission intensity map obtained by filtering the CL signal recorded while scanning the sample in the 3.65–4.13 eV energy window (300–340 nm). A weak, diffuse luminescence appears across the whole flake, accompanied by an individual intense emission localized on a ~80 nm wide spot. No specific structural inhomogeneities corresponding to these emissions can be identified in the HAADF image. In a second step, thanks to the high spatial resolution of the STEM microscope, we illuminated solely the bright spot (white rectangle in Figure 1a–b) while acquiring the CL second order correlation function. The appearance of an antibunching dip with $g^{(2)}(0) = 0.43$ indicates clearly the presence of a single-photon source (Figure 1) with a lifetime of about 2.5 ns as derived from the dip width.

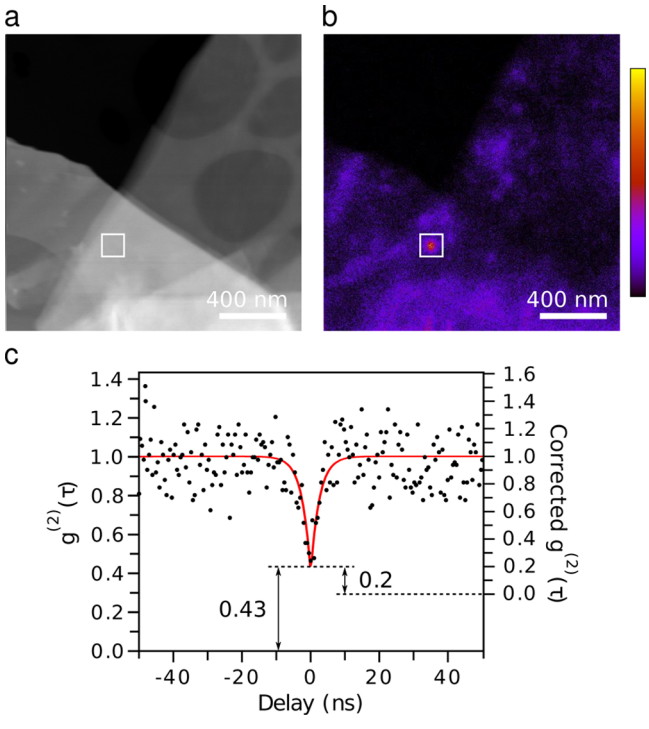

Figure 1. (a) HAADF image of an *h*-BN flake supported by a holey carbon film. (b) Energy-filtered CL intensity map (energy window 3.65–4.13 eV), showing a highly spatially localized (~80 nm) emission spot. (c) Second-order correlation function acquired while illuminating the square region indicated around the emission spot; the left vertical axis refers to the raw data, the right axis to background corrected data. The $g^{(2)}(0) = 0.2$ antibunching dip is the clear signature of a UV single photon emission source with a 2.5 ns lifetime as derived from the dip width.

Exposure times and therefore signal-to-noise ratio were limited by background luminescence associated with irradiation damage as will be discussed later. However, the detection rate was as high as 6×10^4 photon/s per photomultiplier tube (see methods) allowing a $g^{(2)}(0)$ signal-to-noise ratio higher than 5 for reduced exposure times (6 s for the curve in Figure 1). The source therefore appears extremely bright: this detection rate is at least a factor of 4 larger than those obtained for individual NV^0 centers using a similar experimental setup and comparable illumination conditions.[3]

A further step toward the characterization of the midbandgap emission can be achieved by CL hyperspectral imaging at subwavelength spatial resolution (see methods). In Figure 2 we present postprocessing analysis from a CL hyper-spectral image obtained from an individual *h*-BN flake (64 × 64 spectra sequentially acquired while scanning the sample with an 18 nm step size). The HAADF image in Figure 2a demonstrates the fairly uniform thickness of a large part of the scanned region (contrast variations arise mainly from the lacey carbon film on top of which the flake lies). In Figure 2b we present an example spectrum extracted from the hyper-spectral image corresponding to the red rectangle indicated in Figure 2a. As discussed by a number of authors, this structured luminescence can be decomposed into a broad signal centered at 3.9 eV on which a series of sharp lines might be superposed depending on the *h*-BN sample purity.[35] Whereas our experiments were conducted with the sample at about 150 K, it has been demonstrated that these emissions are stable up to temperatures of several hundred degrees.[35,36] The sharp peaks, which have a constant energy separation of about 180 meV, have been ascribed to a 4.09 eV zero-phonon line followed by LO-TO phonon replica.[37−40] Faint shoulders 70 meV below each major line were attributed to additional ZO phonon modes.[40] Whereas in the overall hyper-spectral image we observe strong variations in individual peak intensities, neither relevant energy shifts nor changes in peak shapes have been detected. The local weight of individual spectral features has been extracted through a multigaussian fitting routine applied to each spectrum individually; the structure of the broadband emission has been reproduced by a two-Gaussians fitting function. Maps of the spatial distribution of individual spectral components are presented in Figure 2c–f. The strong spatial correlation of emission spots associated with the 3.73, 3.91, and 4.09 eV peaks demonstrates their unique origin, providing a further experimental confirmation for the phonon replica hypothesis. Highly localized spots (~80 nm) can also be identified in the broadband luminescence map, but a diffuse, weak emission is more extensively observed (Figure 1b and Figure 2c). It should

DOI: 10.1021/acs.nanolett.6b01368
Nano Lett. 2016, 16, 4317–4321

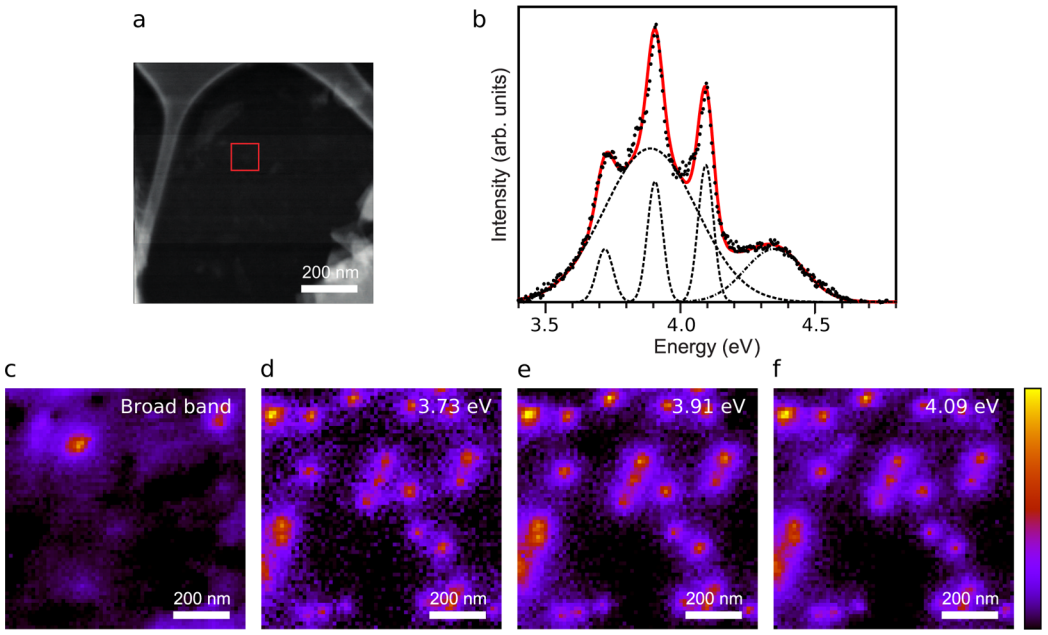

Figure 2. (a) HAADF image of an *h*-BN flake on a lacey carbon grid. (b) Example CL spectrum acquired by integrating the recorded hyperspectral image in the region indicated by the red rectangle in the HAADF image. (c–f) CL intensity maps of the peaks at 3.73, 3.91, and 4.09 eV, showing a perfect spatial match and therefore a unique origin.

be mentioned that where the midbandgap spots are intense the excitonic emissions are strongly quenched or even totally absent.

In Figure 3a we report the cathodoluminescence spectrum corresponding to the bright spot in Figure 1b acquired prior to the $g^{(2)}(\tau)$ measurements in Figure 1c. The HBT integrated

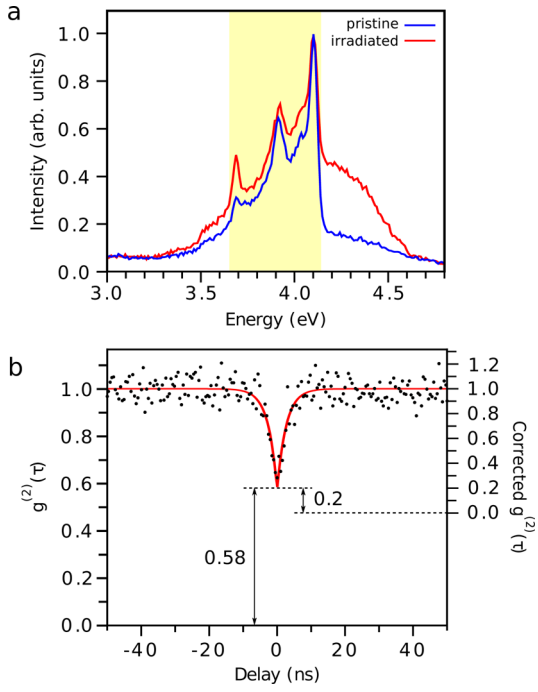

Figure 3. (a) CL emission spectra collected at the bright spot region of Figure 1b, prior and after extended electron irradiation. The shadowed area indicates the energy window selected for the HBT experiment. (b) Second-order correlation function acquired after irradiation; left vertical axis refer to the raw data, right axis to background corrected data.

energy window is indicated by the shadowed region, showing that both the broadband and sharp peak components contribute to the measured $g^{(2)}(\tau)$ function. However, the spatially diffuse broadband corresponds to a background of the effective single photon emission due to the sharp peaks, and therefore it reduces the dip in the $g^{(2)}$ function. A major advantage of performing HBT in a STEM+CL setup is the ability to maximize the signal-to-background ratio (SBR) via a very local illumination of individual color centers. Furthermore, the knowledge of the exact spectral signature at the illuminated area permits one to separate individual spectral components and therefore to evaluate precisely the SBR. In our case, the SBR was extracted using the multigaussian fitting methodology illustrated before. We finally obtain a background-corrected $g^{(2)}(0) = 0.2$ (right vertical scale in Figure 1c), which is almost the minimum attainable value considering the temporal sampling of the experimental setup.

The red curve in Figure 3a corresponds to the CL spectrum of the same area obtained after 150 s of continuous electron illumination. A strong enhancement of the broadband emission is clearly visible. The overall antibunching character of the correlation function is not affected by the prolonged illumination, whereas a decreased SBR leads to a higher $g^{(2)}(0) = 0.58$ (Figure 3b). However, after background subtraction a $g^{(2)}(0) = 0.2$ can be retrieved (Figure 3b). This demonstrates that the two emissions can be attributed to two different sources, one of them, the peaked emission, being an SPE which is not affected by electron irradiation. Whereas the $g^{(2)}(\tau)$ signal-to-noise ratio can be improved by extended exposure times (higher electron doses), an upper limit is ultimately given by the associated decrease in the SBR.

These results indicate that the broadband luminescence, always observed in low-quality crystals, is not associated with extrinsic defects but unequivocally with intrinsic defects that can be generated by electron irradiation. Furthermore, time- and energy-resolved photoluminescence experiments have shown that the long lifetimes (22–200 ns) and multiple

DOI: 10.1021/acs.nanolett.6b01368
Nano Lett. 2016, 16, 4317–4321

decay behavior of the broadband emission is compatible with recombination at donor−acceptor pairs.[39] A number of transmission electron microscopy experiments have imaged the formation of atomic vacancies in monolayer *h*-BN, mostly primary boron vacancies.[41,42] In multilayer *h*-BN structures the ejected atoms can be trapped as interstitials in between the layers. First principle simulations have demonstrated that boron vacancies act as acceptors, whereas boron interstitials or nitrogen vacancies are electron donors.[43,44] Therefore, native or irradiation-generated vacancy-interstitial pairs, or the interaction between different kinds of vacancies, could be compatible with the observed donor−acceptor character of the broadband emission.

Concerning the 4.09 eV peak, its high spatial localization associated with its SPE character indicates unequivocally a point-defect origin. Several experimental works provide convergent evidence that this emission line is associated with a carbon substitutional impurity at a nitrogen site (C_N) which might be easily incorporated during the crystal growth.[45−47] However, the recombination mechanism at the origin of this luminescence remains undetermined. The lifetime of this emission has been estimated by time-resolved photoluminescence to be in the 1.1 ns range.[39,48] This fast decay was later confirmed by our team by measuring the bunching peak decay curve in the autocorrelation function of the cathodoluminescence intensity.[49] Whereas the antibunching signature characterizes a single emission center, bunching occurs for an ensemble of individual centers excited by fast electrons. This can explain the discrepancy between decay times estimated through antibunching and bunching: antibunching provides information on the lifetime of individual centers, which may vary from center to center due to minor structural changes; bunching (as well as time-resolved photoluminescence) averages the decay times of an ensemble of centers, fast events have a dominant effect and multiple close decay times can be not easily separated.

In this work we employed an original setup combining nanometer-resolved CL in a STEM microscope with HBT interferometry to identify a new UV-SPE in *h*-BN. The quantum character of the emission associated with its extremely high spatial localization indicates a point defect origin. These results provide a further experimental confirmation for a previously reported model implicating carbon substitutional atoms at nitrogen sites as the source of this luminescence. An additional broad band, spatially localized but not correlated with the SPE emission, can also be observed in the same energy range. The intensity of this broad band increases upon electron irradiation and therefore vacancies and interstitial defects probably play a role in it. This signal represents a background in the $g^{(2)}(\tau)$ of the SPE which can be easily subtracted using CL spectra recorded aside the autocorrelation function. The high quantum efficiency of the UV-SPE source identified in this work (possibly related to 2D confinement in *h*-BN), its temperature stability and its easiness to obtain in a cheap and environmentally friendly material indicate a considerable technological potential. Finally, these experiments show how this innovative approach combining STEM-CL+HBT can be extremely effective in the quest for new SPEs in new emerging optical materials.

Methods. *Synthesis.* Few-layer hexagonal boron nitride flakes were obtained by chemical exfoliation of commercially available micrometric powder following the protocol presented in ref 50. A solution of 10 mg of *h*-BN powder in 10 mL of isopropanol was sonicated for 10 h and then centrifugated for 120 min at 500 rpm. The supernatant was then dropped on a TEM lacey carbon grid. Flakes presented a lateral size of few microns and an average thickness of few tenths of a nanometer.

Cathodoluminescence. Cathodoluminescence were performed in a dedicated VG-HB501 scanning transmission electron microscope operating at 60 keV, below the atomic displacement threshold for *h*-BN in order to limit irradiation damage. The microscope was provided with a liquid nitrogen cooling system for the sample stage (150 K). The luminescence signal was collected by a parabolic mirror and sent to an optical spectrometer with a 300-groove diffraction grating blazed at 300 nm. The resolution of the spectrometer CCD was 0.17 nm/pixel. Hyperspectral images were obtained by sequentially recording one full CL spectrum per pixel while scanning the sample with a nanometric step size.

HBT. The CL signal collected by the parabolic mirror was guided to a Hanbury−Brown and Twiss interferometer using an optical multimode fiber (600 μm diameter core). Incoming light was filtered using an optical filter in the 300−340 nm wavelength range. We employed lenses covered with a coating optimized for the UV range (290−370 nm) and a beam splitter working in the range of 250−400 nm. Single photons were detected by two photomultiplier (PMT) modules. Time-delay histograms (which are proportional to the second-order correlation function) were acquired using Time-Harp correlation electronics from Picoquant. The typical room background noise varied from 200 to 500 count/s per PMT. Energy-filtered images were acquired by measuring the PMT count rate. Time-delay histograms were normalized to one for $\tau \gg 0$, which is justified by the absence of correlation at a long time delay.

AUTHOR INFORMATION

Corresponding Author

*E-mail: alberto.zobelli@u-psud.fr.

Notes

The authors declare no competing financial interest.

ACKNOWLEDGMENTS

The authors acknowledge support from the Agence Nationale de la Recherche (ANR) program of future investment TEMPOS-CHROMATEM (No. ANR-10-EQPX-50). The work has also received funding from the European Union in Seventh Framework Programme (No. FP7/2007−2013) under Grant Agreement No. n312483 (ESTEEM2).

REFERENCES

(1) Brouri, R.; Beveratos, A.; Poizat, J. P.; Grangier, P. *Opt. Lett.* **2000**, *25*, 1294−6.

(2) Mizuochi, N.; Makino, T.; Kato, H.; Takeuchi, D.; Ogura, M.; Okushi, H.; Nothaft, M.; Neumann, P.; Gali, A.; Jelezko, F.; Wrachtrup, J.; Yamasaki, S. *Nat. Photonics* **2012**, *6*, 299−303.

(3) Tizei, L. H. G.; Kociak, M. *Phys. Rev. Lett.* **2013**, *110*, 153604.

(4) Castelletto, S.; Johnson, B. C.; Ivády, V.; Stavrias, N.; Umeda, T.; Gali, A.; Ohshima, T. *Nat. Mater.* **2013**, *13*, 151−156.

(5) Castelletto, S.; Johnson, B. C.; Zachreson, C.; Beke, D.; Balogh, I.; Ohshima, T.; Aharonovich, I.; Gali, A. *ACS Nano* **2014**, *8*, 7938−7947.

(6) Tonndorf, P.; Schmidt, R.; Schneider, R.; Kern, J.; Buscema, M.; Steele, G. A.; Castellanos-Gomez, A.; van der Zant, H. S. J.; de Vasconcellos, S. M.; Bratschitsch, R. *Optica* **2015**, *2*, 347−352.

(7) Srivastava, A.; Sidler, M.; Allain, A. V.; Lembke, D. S.; Kis, A.; Imamoğlu, A. *Nat. Nanotechnol.* **2015**, *10*, 491−496.

DOI: 10.1021/acs.nanolett.6b01368
Nano Lett. 2016, 16, 4317−4321

(8) He, Y.-M.; Clark, G.; Schaibley, J. R.; He, Y.; Chen, M.-C.; Wei, Y.-J.; Ding, X.; Zhang, Q.; Yao, W.; Xu, X.; Lu, C.-Y.; Pan, J.-W. *Nat. Nanotechnol.* **2015**, *10*, 497−502.
(9) Koperski, M.; Nogajewski, K.; Arora, A.; Cherkez, V.; Mallet, P.; Veuillen, J.-Y.; Marcus, J.; Kossacki, P.; Potemski, M. *Nat. Nanotechnol.* **2015**, *10*, 503−506.
(10) Chakraborty, C.; Kinnischtzke, L.; Goodfellow, K. M.; Beams, R.; Vamivakas, A. N. *Nat. Nanotechnol.* **2015**, *10*, 507−511.
(11) Tran, T. T.; Bray, K.; Ford, M. J.; Toth, M.; Aharonovich, I. *Nat. Nanotechnol.* **2015**, *11*, 37−41.
(12) Tran, T. T.; Zachreson, C.; Berhane, A. M.; Bray, K.; Sandstrom, R. G.; Li, L. H.; Taniguchi, T.; Watanabe, K.; Aharonovich, I.; Toth, M. *Phys. Rev. Appl.* **2016**, *5*, 034005.
(13) Tran, T. T.; ElBadawi, C.; Totonjian, D.; Lobo, C. J.; Grosso, G.; Moon, H.; Englund, D. R.; Ford, M. J.; Aharonovich, I.; Toth, M. *arXiv*:1603.09608, **2016**.
(14) Jungwirth, N. R.; Calderon, B.; Ji, Y.; Spencer, M. G.; Flatté, M. E.; Fuchs, G. D. *arXiv*:1605.04445, 2016.
(15) Buttler, W.; Hughes, R.; Kwiat, P.; Lamoreaux, S.; Luther, G.; Morgan, G.; Nordholt, J.; Peterson, C.; Simmons, C. *Phys. Rev. Lett.* **1998**, *81*, 3283.
(16) Ursin, R.; et al. *Nat. Phys.* **2007**, *3*, 481−486.
(17) Xu, Z.; Sadler, B. M. *IEEE Commun. Mag.* **2008**, *46*, 67−73.
(18) Kako, S.; Santori, C.; Hoshino, K.; Götzinger, S.; Yamamoto, Y.; Arakawa, Y. *Nat. Mater.* **2006**, *5*, 887−892.
(19) Santori, C.; Götzinger, S.; Yamamoto, Y.; Kako, S.; Hoshino, K.; Arakawa, Y. *Appl. Phys. Lett.* **2005**, *87*, 051916.
(20) Kim, J.-H.; Ko, Y.-H.; Gong, S.-H.; Ko, S.-M.; Cho, Y.-H. *Sci. Rep.* **2013**, *3*.10.1038/srep02150
(21) Holmes, M. J.; Choi, K.; Kako, S.; Arita, M.; Arakawa, Y. *Nano Lett.* **2014**, *14*, 982−986.
(22) Ma, L.; Slattery, O.; Tang, X. *Phys. Rep.* **2012**, *521*, 69−94.
(23) Taylor, C., II; Brown, S.; Subramaniam, V.; Kidner, S.; Rand, S.; Clarke, R. *Appl. Phys. Lett.* **1994**, *65*, 1251−1253.
(24) Watanabe, K.; Taniguchi, T. *Phys. Rev. B: Condens. Matter Mater. Phys.* **2009**, *79*, 193104.
(25) Watanabe, K.; Taniguchi, T. *Int. J. Appl. Ceram. Technol.* **2011**, *8*, 977−989.
(26) Watanabe, K.; Taniguchi, T.; Kanda, H. *Nat. Mater.* **2004**, *3*, 404−409.
(27) Bourrellier, R.; Amato, M.; Galvão Tizei, L. H.; Giorgetti, C.; Gloter, A.; Heggie, M. I.; March, K.; Stéphan, O.; Reining, L.; Kociak, M.; Zobelli, A. *ACS Photonics* **2014**, *1*, 857−862.
(28) Cassabois, G.; Valvin, P.; Gil, B. *Nat. Photonics* **2016**, *10*, 262−262.
(29) Cassabois, G.; Valvin, P.; Gil, B. *Phys. Rev. B: Condens. Matter Mater. Phys.* **2016**, *93*, 035207.
(30) Katzir, A.; Suss, J. T.; Zunger, A.; Halperin, A. *Phys. Rev. B* **1975**, *11*, 2370−2377.
(31) Zagonel, L. F.; Mazzucco, S.; Tencé, M.; March, K.; Bernard, R.; Laslier, B.; Jacopin, G.; Tchernycheva, M.; Rigutti, L.; Julien, F. H.; Songmuang, R.; Kociak, M. *Nano Lett.* **2011**, *11*, 568−573.
(32) Ponce, F. A.; Bour, D. P.; Gotz, W.; Wright, P. J. *Appl. Phys. Lett.* **1996**, *68*, 57−59.
(33) Hanbury Brown, R.; Twiss, R. Q. *Nature* **1956**, *178*, 1046−1048.
(34) Tizei, L. H. G.; Meuret, S.; Nagarajan, S.; Treussart, F.; Fang, C.-Y.; Chang, H.-C.; Kociak, M. *Phys. Status Solidi A* **2013**, *210*, 2060−2065.
(35) Larach, S.; Shrader, R. E. *Phys. Rev.* **1956**, *104*, 68−73.
(36) Du, X.; Li, J.; Lin, J.; Jiang, H. *Appl. Phys. Lett.* **2015**, *106*, 021110.
(37) Kuzuba, T.; Era, K.; Ishii, T.; Sato, T.; Iwata, M. *Physica B+C* **1981**, *105*, 339−342.
(38) Museur, L.; Anglos, D.; Petitet, J.-P.; Michel, J.-P.; Kanaev, A. V. *J. Lumin.* **2007**, *127*, 595−600.
(39) Museur, L.; Feldbach, E.; Kanaev, A. *Phys. Rev. B: Condens. Matter Mater. Phys.* **2008**, *78*, 155204.
(40) Vuong, T.; Cassabois, G.; Valvin, C.; Chassagneux, Y.; Voisin, C.; Gil, B., submitted.
(41) Jin, C.; Lin, F.; Suenaga, K.; Iijima, S. *Phys. Rev. Lett.* **2009**, *102*, 195505.
(42) Meyer, J. C.; Chuvilin, A.; Algara-Siller, G.; Biskupek, J.; Kaiser, U. *Nano Lett.* **2009**, *9*, 2683−2689.
(43) Orellana, W.; Chacham, H. *Phys. Rev. B: Condens. Matter Mater. Phys.* **2001**, *63*, 125205.
(44) Attaccalite, C.; Bockstedte, M.; Marini, A.; Rubio, A.; Wirtz, L. *Phys. Rev. B: Condens. Matter Mater. Phys.* **2011**, *83*, 144115.
(45) Moore, A.; Singer, L. *J. Phys. Chem. Solids* **1972**, *33*, 343−356.
(46) Katzir, A.; Suss, J.; Zunger, A.; Halperin, A. *Phys. Rev. B* **1975**, *11*, 2370−2377.
(47) Taniguchi, T.; Watanabe, K. *J. Cryst. Growth* **2007**, *303*, 525−529.
(48) Era, K.; Minami, F.; Kuzuba, T. *J. Lumin.* **1981**, *24*, 71−74.
(49) Meuret, S.; Tizei, L. H. G.; Cazimajou, T.; Bourrellier, R.; Chang, H. C.; Treussart, F.; Kociak, M. *Phys. Rev. Lett.* **2015**, *114*, 197401.
(50) Coleman, J. N.; et al. *Science* **2011**, *331*, 568−571.

DOI: 10.1021/acs.nanolett.6b01368
Nano Lett. 2016, 16, 4317−4321